

Kinetic Modeling of the Tau PET Tracer ^{18}F -AV-1451 in Human Healthy Volunteers and Alzheimer's Disease Subjects

Olivier Barret¹, David Alagille¹, Sandra Sanabria², Robert A. Comley³, Robby M. Weimer², Edilio Borroni³, Mark Mintun⁴, Nicholas Seneca⁵, Caroline Papin¹, Thomas Morley¹, Ken Marek¹, John P. Seiby¹, Gilles D. Tamagnan¹, Danna Jennings¹

¹ Molecular NeuroImaging LLC, 60 Temple Street, New Haven, CT, 06510, USA

² Genentech Research and Early Development, Genentech, 1 DNA Way, South San Francisco, CA, 94080, USA

³ Pharma Research and Early Development, F. Hoffmann-La Roche, Konzern-Hauptsitz, Grenzacherstrasse 124, CH-4070 Basel, Switzerland

⁴ Avid Radiopharmaceuticals, 3711 Market St. Philadelphia, PA, 19104, USA

⁵ Product Development, F. Hoffmann-La Roche, Konzern-Hauptsitz, Grenzacherstrasse 124, CH-4070 Basel, Switzerland

Name and Address for Correspondence:

Olivier Barret, PhD
Molecular NeuroImaging, LLC
60 Temple Street, Suite 8B
New Haven, CT
USA

Telephone: 203-401-4317

Fax: 203-789-8037

Email: obarret@mnimaging.com

Word count: 4,997 words

RUNNING TITLE: Modeling of ^{18}F -AV-1451 in humans

ABSTRACT

^{18}F -AV-1451 is currently the most widely used of several experimental tau PET tracers. The objective of this study was to evaluate ^{18}F -AV-1451 binding with full kinetic analysis using a metabolite corrected arterial input function, and to compare parameters derived from kinetic analysis with standardized uptake value ratio (SUVR) calculated over different imaging time intervals.

Methods ^{18}F -AV-1451 PET brain imaging was completed in 16 subjects: 4 young healthy volunteers (YHV), 4 aged healthy volunteers (AHV) and 8 Alzheimer's disease subjects (AD). Subjects were imaged for 3.5 hours, with arterial blood samples obtained throughout. PET data were analyzed using plasma and reference-tissue-based methods to estimate the distribution volume (V_T), the binding potential (BP_{ND}) and SUVR. BP_{ND} and SUVR were calculated using cerebellar cortex as reference region and were compared across the different methods and across the three groups (YHV, AHV and AD).

Results: AD demonstrated increased ^{18}F -AV-1451 retention compared to HV based on both invasive and non-invasive analyses in cortical regions where paired helical filaments (PHF) tau accumulation is expected in AD. A correlation of $R^2 > 0.93$ was found between BP_{ND} (130 min) and SUVR-1 at all time intervals. Cortical SUVR curves reached a relative plateau around 1.0-1.2 for YHV and AHV by ~50 min, but increased in AD by up to ~20% at 110-130 min and ~30% at 160-180min relative to 80-100min. V_T (130 min) was lower by 30-35% in the YHV compared to AHV.

Conclusions Our data suggest that although ^{18}F -AV-1451 SUVR curves do not reach a plateau and are still increasing in AD, an SUVR calculated over imaging window of 80-100 min (as currently used in clinical studies) provides estimates of PHF tau burden in good correlation with BP_{ND} , while SUVR sensitivity to regional cerebral blood changes needs further investigation.

Keywords: Tau protein, Alzheimer, PET, ^{18}F -AV-1451, kinetic modeling

INTRODUCTION

The accumulation of folded hyper-phosphorylated tau is one pathologic hallmark for Alzheimer's disease and forms the basis of the neuropathological staging of Alzheimer-related pathology in the brain (1). ^{18}F -AV-1451 (synonyms ^{18}F -T807, flortaucipir) (2) is a PET radiotracer with high affinity and specificity for tau aggregates, while lacking affinity for concomitant amyloid- β plaques in human AD (3, 4). Several additional PET agents have been proposed for the imaging of tau in the brain, in particular ^{11}C -PBB3 (5, 6), ^{18}F -THK-5117 (7), ^{18}F -T808 (8), ^{18}F -PI-2014 (9) and more recently ^{11}C -RO6924963, ^{11}C -RO6931643, ^{18}F -RO6958948 (10), ^{18}F -THK-5351 (11), ^{18}F -GTP1 (12) and ^{18}F -MK6240 (13), and have been or are being characterized and evaluated in humans. Currently, ^{18}F -AV-1451 has been the most widely used and characterized PET tracer (2-4, 14, 15) in clinical studies. Early clinical evaluation has demonstrated heterogeneous and asymmetric brain uptake of the radiotracer (2) consistent with the earlier reports by Braak and Braak (1) showing distribution of tau that follows discrete patterns in cross-sectional postmortem analyses generally correlating with AD severity.

Validation of a quantitative PET outcome measure for ^{18}F -AV-1451 is necessary to address questions relevant to drug development and the primary pathophysiology of AD. SUVR has been widely utilized as a semi-quantitative outcome measure, because it can be obtained using simplified methods of acquisition and analysis. Quantification using this method may be influenced by confounding factors such that assessment of ^{18}F -AV-1451 signal and/or longitudinal changes of signal may not solely reflect the actual tau density in brain tissue.

In this report, we have compared the validity of SUVR to more robust quantitative measurements obtained through kinetic modeling of the PET data. Recently, SUVR was compared to a tissue-based method (15). In this study, an arterial input

function corrected for metabolites was obtained in both HV and AD, and classic pharmacokinetic modeling of the ^{18}F -AV-1451 PET data using plasma-based or tissue-based methods was performed.

MATERIALS AND METHODS

Radiochemistry

Radiolabeling and preparation of ^{18}F -AV-1451 was described previously (16). All productions showed radiochemical purity above 99% and specific activity exceeding 200 GBq/ μmol . The average decay-corrected radiochemical yield was $15.4 \pm 5.5\%$ (n = 16) in 60 min.

Human Subjects

Sixteen subjects were enrolled and completed ^{18}F -AV-1451 brain PET studies: 4 YHV (age 26-37), 4 AHV (age 51-72) and 8 AD (age 57-85, Mini-Mental State Examination (MMSE) 14-29) (Table 1). All subjects gave their written informed consent before participation in this study. The study protocol was reviewed and approved by the New England Institutional Review Board. The study was registered on ClinicalTrials.gov (NCT02370524).

Individuals with mild and moderate AD were required to meet the criteria based on the National Institute of Neurological and Communicative Disorders and Stroke/Alzheimer's Disease and Related Disorders Association and Diagnostic and Statistical Manual of Mental Disorders (17) for study eligibility. All HV were required to have no evidence of cognitive impairment or early dementia as judged by the investigator. AHV and AD underwent ^{18}F -Florbetapir amyloid imaging at screening and required a visual analysis positive for AD (18) and negative for AHV.

Brain PET Studies

PET images were acquired on a Siemens ECAT EXACT HR+ camera. Subjects were administered intravenously a single dose of ^{18}F -AV-1451 (details are provided in Table 1) over 2 min, followed by a 10 mL saline flush.

Dynamic 3D brain PET images were acquired over 210 min as three imaging sessions of 50 min each (0-50 min, 80-130 min and 160-210 min) with 30 min breaks between sessions. The first session consisted of 21 frames (6 x 0.5 min, 4 x 1 min, 4 x 2 min, 7 x 5 min) and the second and third session consisted of 10 frames (10 x 5 min). A ^{68}Ge rod source transmission scan was obtained before each emission for attenuation correction. PET data were corrected for randoms, dead time, scatter and attenuation and PET images were reconstructed using ordered subset expectation maximization algorithm (4 iterations, 16 subsets, 5 mm Gaussian post filter).

A structural 3D T1-weighted magnetic resonance image (MRI) was acquired for all subjects on a Siemens Espree 1.5-T scanner (MPRAGE; inversion time, 1.1 s; repetition time, 1.97 s; echo time, 3.17 ms; flip angle, 15°).

Blood Sampling and Analysis

Arterial blood samples were collected throughout the 210 min of acquisition (every 30 seconds until 4 minutes post-injection with decreasing frequency thereafter) and whole blood and plasma radioactivity measured in a well-type γ -counter (Perkin Elmer Wallac 2480, USA). Radio-metabolites were measured in a subset of samples (4, 8, 15, 30, 60, 90, 130, 170 and 210 min) by reverse-phase high performance liquid chromatography, and plasma protein binding free fraction (f_p) was measured by ultrafiltration (Centrifree®, Millipore).

The parent fraction profile was fitted with a mono-exponential plus constant function using measurements up to 130 min (last two samples at 170 min and 210 min

suffered from low count statistics and were excluded from the fit), and extrapolated thereafter. The arterial plasma concentration curve was time multiplied by the fitted curve to correct for radio-metabolites.

Image Processing and Analysis

Images were analyzed in PMOD 3.607 software (PMOD Technologies, Zurich, Switzerland). All realignment procedures used normalized mutual information. PET images were motion-corrected within and between imaging sessions by realigning each image to the initial flow-like (15 min) average image. The subject MRI was segmented into grey and white matter maps. The initial flow-like average PET image was used to align the whole PET series onto the MRI, and subsequently both MRI and PET series were spatially normalized to the standard Montreal Neurologic Institute space. Hammers volume of interest atlas (19) was applied to normalized PET images and time activity curves were extracted for the following brain regions (left and right side regions separately): frontal (middle, inferior, superior), parietal, occipital, temporal (superior lateral, inferior lateral, mesial), putamen, caudate nucleus, globus pallidus, thalamus as well as cerebellar cortex, with cortical and cerebellar cortex regions constrained to grey matter voxels. The cerebellar cortex region was eroded away from other regions by 8 mm to minimize spill-over, in particular from the temporal and occipital regions.

The standard 2-tissue compartment model (2T), one-tissue compartment model (1T) and Logan graphical analysis (LGA; $t^* = 80$ min) plasma-based methods were used with the radio-metabolite corrected arterial plasma input function to estimate V_T in specific brain regions (20, 21). 1T and 2T used a fixed blood volume of 5%. BP_{ND} was calculated indirectly as $(V_T - V_{ND})/V_{ND}$, where V_{ND} is the non-displaceable volume of distribution as estimated in the cerebellar cortex. The non-invasive simplified reference tissue model (SRTM) (22) and non-invasive Logan Graphical Analysis (NI-LGA; $k_2' =$

0.05 min⁻¹, $t^* = 80$ min) (21) were used to determine directly BP_{ND} using the cerebellar cortex as the reference region. For NI-LGA, k_2' was fixed to the average value across regions and subjects of k_2' calculated with SRTM. V_T and BP_{ND} were estimated for 130 min (first two imaging sessions) and 210 min of data (whole acquisition), and unless specified otherwise the reported results are for 130 min due to the increased input function uncertainty and PET data noise at later times.

Standardized uptake values (SUV) were calculated by normalizing the uptake values by the injected dose divided by the subject weight. Target to cerebellar cortex SUVR were calculated for four time intervals (80-100 min, 110-130 min, 160-180 min and 190-210 min), and compared to BP_{ND} .

RESULTS

Representative average ¹⁸F-AV-1451 SUVR images (80-100 min) are shown in Fig.1 for one YHV, one AHV and three AD, visually demonstrating increased retention in AD compared to HV. Time activity and SUVR curves are shown in Fig. 2 for one YHV, one AHV and one AD. YHV and AHV display rapid uptake and clearance of the tracer across all brain regions, with putamen uptake slightly elevated initially in YHV and clearly elevated in AHV. Retention of the tracer is observed in AD in cortical regions with noticeable region-specific and asymmetrical signal, with further elevated putamen uptake exhibiting very different kinetic compared to cortical regions with high initial uptake and much faster clearance. Pseudo-equilibrium is not reached at 210 min post injection with SUVR curves still increasing. Additional across subject comparison of SUVR curves per region are provided in Supplemental Figs. 1-6.

Moderately fast metabolism of ¹⁸F-AV-1451 was observed (Fig. 3A), with two main radio-metabolites much more polar than the parent. At 90 min post-radiotracer injection, the parent fraction in arterial plasma was $17.3 \pm 7.0\%$ across all subjects ($n =$

16). No difference was observed between the three groups. The free fraction in plasma (f_p) was low at $0.19 \pm 0.12\%$ ($n=16$). The average metabolite corrected arterial plasma is also shown in Fig. 3B.

Examples of fits/linear regression for 210 min of data are shown in Fig. 4 for an AD. 2T described adequately the data up to 210 min. 1T gave poor fits for all subjects and regions, including the cerebellar cortex (data not shown) and is not reported further. LGA or NI-LGA plots are close to linearity for the last two imaging sessions. SRTM did not describe the data as well over 210 min, with some convergence/fit difficulties in some regions, while showing excellent agreement with NI-LGA ($R^2 > 0.99$, linear regression on top of identity line), and is therefore not reported further.

Detailed results of the 2T analysis are given in Table 2 and Fig. 5. K_1 was regionally different, highest in the putamen, but appeared similar in YHV and AHV in all regions (within $\sim 3\%$), and across the three groups in the cerebellar cortex and putamen, while lower by $\sim 10-15\%$ in the cortical regions of AD, similar to previous findings (23). K_1/k_2 was clearly lower by $\sim 30\%$ in YHV including in the cerebellar cortex (2.7 mL/cm^3) compared to AHV (3.9 mL/cm^3) and AD (3.7 mL/cm^3). V_T was elevated in the cortical regions of AD (as expected), but similar between AHV and AD in the cerebellum (6.0 and 5.9 mL/cm^3 , respectively), while noticeably lower by again $30-35\%$ in YHV with 4.1 mL/cm^3 for the cerebellar cortex. A regression analysis (Fig. 6) showed a correlation between V_T and the subjects age with an $R^2 > 0.87$ ($n=8$, YHV and AHV), and a higher increase with age in the putamen (slope of ~ 0.095) compared to other regions (slope of $\sim 0.06-0.08$). K_1 and V_T were well identified, with parameter errors of $2-4\%$. The identifiability for k_2 was decreased (error up to $\sim 7\%$) but the ratio K_1/k_2 maintained an acceptable error of $\sim 4\%$, except in the mesial temporal and putamen. k_3 and k_4 were not well identified (errors up to $\sim 25\%$), in particular for k_3 in the mesial temporal and putamen ($30-35\%$), while k_3/k_4 was better defined ($\sim 10\%$), except in the mesial temporal

and putamen (15-25%), where the increased errors in these regions is likely caused by higher correlation between k_2 and k_3 (24).

Results of BP_{ND} and SUVR are summarized in Supplemental Table 1, and correlation analyses between these measurements in cortical regions (AD only) are provided in Table 3 and shown in Fig. 7. Overall, a good correlation was found between all methods and scan durations with $R^2 > 0.96$. LGA and NI-LGA underestimates BP_{ND} by ~10% and ~20%, respectively, compared to 2T. The agreement between 2T and SUVR-1 in terms of R^2 was similar for (80-100 min) and (110-130 min), while slightly better for (110-130 min) when compared to LGA or NI-LGA estimates, although when additionally considering a slope closer to unity and a smaller bias (introduced through the intercept) the (110-130 min) interval performed better. Within-method comparison showed a time-dependency of the estimates, with BP_{ND} increasing by 15%, 10% and 12% for 2T, LGA and NI-LGA, respectively and V_T increasing by ~20% for both 2T and LGA (with a higher R^2 for the graphical methods) when using 210 min of data, likely due to non-equilibrium between plasma and brain regions. LGA V_T correlated strongly with 2T ($R^2 > 0.98$), with however an underestimation of ~5%.

DISCUSSION

We report the kinetic analysis of ^{18}F -AV-1451 using an arterial input function to evaluate its pharmacokinetic properties in brain. AD demonstrated increased ^{18}F -AV-1451 retention compared to HV visually in cortical regions where PHF-tau accumulation is expected in AD, as well as quantitatively based invasive (2T and LGA) and non-invasive (NI-LGA and SUVR) analyses. Subjects with presumed negligible or low tau exhibited evidence of equilibration with constant tissue ratios attained, while those with presumed substantial tau showed steady accumulation beyond 210 min. Despite these kinetic characteristics, a comparison between invasive 2T model and SUVR showed a strong

linear correlation ($R^2 > 0.96$) between BP_{ND} and SUVR-1 across subjects and across regions. Both imaging time intervals of (80-100 min) and (110-130 min) gave comparable results, in agreement with previous findings (25), with a bias $< 10-15\%$ compared to BP_{ND} , although overall the latter (110-130 min) interval performed slightly better. The observed linearity between SUVR and BP_{ND} suggests that SUVR would provide robust estimates across levels of tau for cross sectional or longitudinal imaging studies, although further studies with dynamic image acquisition may be warranted to confirm the linearity of the relationship across a wider range of tau load. In this study, other factors such as the SUVR reproducibility at different time intervals or its sensitivity to blood flow were not taken into consideration. The impact of regional cerebral blood flow changes, likely to happen in AD (26), on SUVR but also BP_{ND} needs further investigation through computer simulations, BP_{ND} being likely less sensitive but requiring dynamic data acquisition not always feasible in clinical studies. Additionally our results highlight the time dependence of SUVR (Fig. 7D), and the scan imaging time should be controlled, particularly in longitudinal or drug development studies, not to introduce additional variability in Δ SUVR assessments.

A different kinetic profile was observed in putamen, globus pallidus and thalamus compared to cortical regions (Supplemental Figs. 5 and 6), suggesting that ^{18}F -AV-1451 may bind to a different site in these regions, with a higher (about double) k_4 than in cortical regions (Table 2). Furthermore, similar to our findings of elevated signal in the putamen and globus pallidus in AHV and AD compared to YHV, an increased SUVR in older subjects was recently reported (27) where it was hypothesized that the higher uptake was due to an increased capillary permeability in the putamen and globus pallidus, but not in the cerebellar cortex. An increased capillary permeability would imply an increased extraction and in turn, under passive transport condition through the blood brain barrier, an increased K_1 and k_2 that would produce an initial higher uptake

(higher K_1) followed by a faster washout (higher k_2). However, our kinetic modeling results showed similar K_1 across the three groups in the putamen and cerebellar cortex with, on the other hand, a lower k_2 (higher K_1/k_2) in AHV and AD compared to YHV.

V_T was increased in AHV and AD not solely in the putamen but in all brain regions investigated, including the cerebellar cortex (Fig. 5 and Table 2). Furthermore, this increase was found to be age dependent (Fig. 6). This age dependent V_T increase appears through the k_2 parameter (negative correlation), although because of parameters identifiability (correlation between k_2 and k_3) (24), was more pronounced for V_T . Although the age dependency mostly normalized out when calculating SUVR or BP_{ND} , with for instance a remaining correlation between the subjects age and SUVR (80-100 min) of $R^2=0.79$ in the putamen ($p<0.001$, increase of 0.0060/year) and of $R^2=0.31$ in the lateral temporal cortex (not significant ($p=0.1$), increase of 0.0017/year), these finding suggests that HV should be age-matched with AD when using SUVR or BP_{ND} since V_T increased in the cerebellar cortex. One interpretation of these results would be of an age dependent increase of non-specific signal or binding to a secondary target not kinetically separated from the non-displaceable signal, although it is not clear what a widespread secondary binding increasing with age would be. Another interpretation would be a change of the tracer efflux to plasma (27), although this would imply some transport mechanism through the blood brain barrier other than passive diffusion.

CONCLUSION

^{18}F -AV-1451 retention is currently assessed in clinical studies of AD at 80-100 minutes after injection. Simplified methods of image acquisition or analysis often require a trade-off between accuracy and simplicity, and given the good correlation between BP_{ND} and SUVR-1, our data suggests that SUVR estimates in this imaging window provide information of tau burden, with an underestimation of 10 to 15% for higher tau load,

although the later imaging window of 110-130 minutes performed slightly better. Consideration should be given to imaging time in longitudinal or drug development studies not to introduce additional variability in the assessment of tau load changes, while SUVR sensitivity to changes in regional cerebral blood or clearance should be further investigated.

ACKNOWLEDGMENTS

We thank Julie C. Price for reading the manuscript and providing suggestions.

DISCLOSURE

This study was sponsored by Molecular Neuroimaging, a division of inviCRO, and funded by Roche. O. Barret, D. Alagille, C. Papin, T. Morley, K. Marek, J. Seibyl, G. Tamagnan, D. Jennings are employees of Molecular Neuroimaging. R. Comley, E. Borroni, N. Seneca are employees of Roche, S. Sanabria, R. Weimer are employees of Genentech, M. Mintun is employee of Avid.

REFERENCES

1. Braak H, Braak E. Neuropathological staging of Alzheimer-related changes. *Acta Neuropathol.* 1991;82:239-259.
2. Chien DT, Bahri S, Szardenings AK, et al. Early clinical PET imaging results with the novel PHF-tau radioligand [F-18]-T807. *J Alzheimers Dis.* 2013;34:457-468.
3. Xia CF, Arteaga J, Chen G, et al. [18F]T807, a novel tau positron emission tomography imaging agent for Alzheimer's disease. *Alzheimers Dement.* 2013;9:666-676.
4. Marquie M, Normandin MD, Vanderburg CR, et al. Validating novel tau positron emission tomography tracer [F-18]-AV-1451 (T807) on postmortem brain tissue. *Ann Neurol.* 2015;78:787-800.
5. Wood H. Alzheimer disease: [11C]PBB3--a new PET ligand that identifies tau pathology in the brains of patients with AD. *Nat Rev Neurol.* 2013;9:599.
6. Maruyama M, Shimada H, Suhara T, et al. Imaging of tau pathology in a tauopathy mouse model and in Alzheimer patients compared to normal controls. *Neuron.* 2013;79:1094-1108.

7. Okamura N, Furumoto S, Harada R, et al. Novel ¹⁸F-labeled arylquinoline derivatives for noninvasive imaging of tau pathology in Alzheimer disease. *J Nucl Med.* 2013;54:1420-1427.
8. Chien DT, Szardenings AK, Bahri S, et al. Early clinical PET imaging results with the novel PHF-tau radioligand [F18]-T808. *J Alzheimers Dis.* 2014;38:171-184.
9. Muhs A, Berndt M, Kroth H, et al. Characterization and development of novel tau PET tracers for the assessment of tau spreading in Alzheimer's disease. *J Prev Alz Dis.* 2015;2:273.
10. Wong DF, Borroni E, Kuwabara H, et al. First in-human PET study of 3 novel tau radiopharmaceuticals: [11C]RO6924963, [11C]RO6931643, and [18F]RO6958948. *Alzheimers Dement.* 2015;11:850-851.
11. Harada R, Okamura N, Furumoto S, et al. ¹⁸F-THK5351: a novel PET radiotracer for imaging neurofibrillary pathology in Alzheimer disease. *J Nucl Med.* 2016;57:208-214.
12. Sanabria Bohorquez S, Barret O, Tamagnan G, et al. Quantification, test-retest and dosimetry of the novel Genentech tau probe 1, [18F]GTP1. *10th Human Amyloid Imaging.* Miami, Florida, USA; 2016:16 (S11-PP43).

13. Walji AM, Hostetler ED, Selnick H, et al. Discovery of 6-(Fluoro-(18)F)-3-(1H-pyrrolo[2,3-c]pyridin-1-yl)isoquinolin-5-amine ([18F]-MK-6240): a positron emission tomography (PET) imaging agent for quantification of neurofibrillary tangles (NFTs). *J Med Chem.* 2016;59:4778-4789.
14. Choi JY, Lyoo CH, Lee JH, et al. Human radiation dosimetry of [(18)F]AV-1451(T807) to detect tau pathology. *Mol Imaging Biol.* 2016;18:479-482.
15. Shcherbinin S, Schwarz AJ, Joshi A, et al. Kinetics of the tau PET tracer 18F-AV-1451 (T807) in subjects with normal cognitive function, mild cognitive impairment, and Alzheimer disease. *J Nucl Med.* 2016;57:1535-1542.
16. Shoup TM, Yokell DL, Rice PA, et al. A concise radiosynthesis of the tau radiopharmaceutical, [18F]T807. *J Labelled Comp Radiopharm.* 2013;56:736-740.
17. McKhann GM, Knopman DS, Chertkow H, et al. The diagnosis of dementia due to Alzheimer's disease: recommendations from the National Institute on Aging-Alzheimer's Association workgroups on diagnostic guidelines for Alzheimer's disease. *Alzheimers Dement.* 2011;7:263-269.

18. Schreiber S, Landau SM, Fero A, Schreiber F, Jagust WJ, Alzheimer's Disease Neuroimaging Initiative. Comparison of visual and quantitative Florbetapir F 18 positron emission tomography analysis in predicting mild cognitive impairment outcomes. *JAMA Neurol.* 2015;72:1183-1190.
19. Hammers A, Allom R, Koepp MJ, et al. Three-dimensional maximum probability atlas of the human brain, with particular reference to the temporal lobe. *Hum Brain Mapp.* 2003;19:224-247.
20. Innis RB, Cunningham VJ, Delforge J, et al. Consensus nomenclature for in vivo imaging of reversibly binding radioligands. *J Cereb Blood Flow Metab.* 2007;27:1533-1539.
21. Logan J. Graphical analysis of PET data applied to reversible and irreversible tracers. *Nucl Med Biol.* 2000;27:661-670.
22. Lammertsma AA, Hume SP. Simplified reference tissue model for PET receptor studies. *Neuroimage.* 1996;4:153-158.
23. Trollor JN, Sachdev PS, Haindl W, Brodaty H, Wen W, Walker BM. Regional cerebral blood flow deficits in mild Alzheimer's disease using high resolution single photon emission computerized tomography. *Psychiatry Clin Neurosci.* 2005;59:280-290.

24. Koeppe RA, Frey KA, Vander Borghet TM, et al. Kinetic evaluation of [11C]dihydrotetrabenazine by dynamic PET: measurement of vesicular monoamine transporter. *J Cereb Blood Flow Metab.* 1996;16:1288-1299.
25. Baker S, Price JC, Lockhart SN, et al. Reference tissue-based kinetic evaluation of [F-18]AV-1451 in aging and dementia. *12th International Conference on Quantification of Brain Function with PET.* Vancouver, Canada; 2015:82 (BRAIN-0848).
26. van Berckel BN, Ossenkuppele R, Tolboom N, et al. Longitudinal amyloid imaging using 11C-PiB: methodologic considerations. *J Nucl Med.* 2013;54:1570-1576.
27. Pascual B, Rockers E, Bajaj S, et al. Regional kinetics of [18F]AV-1451 uptake and Gadolinium concentration in young and older subjects. *10th Human Amyloid Imaging.* Miami, Florida, USA; 2016:170 (PO187).

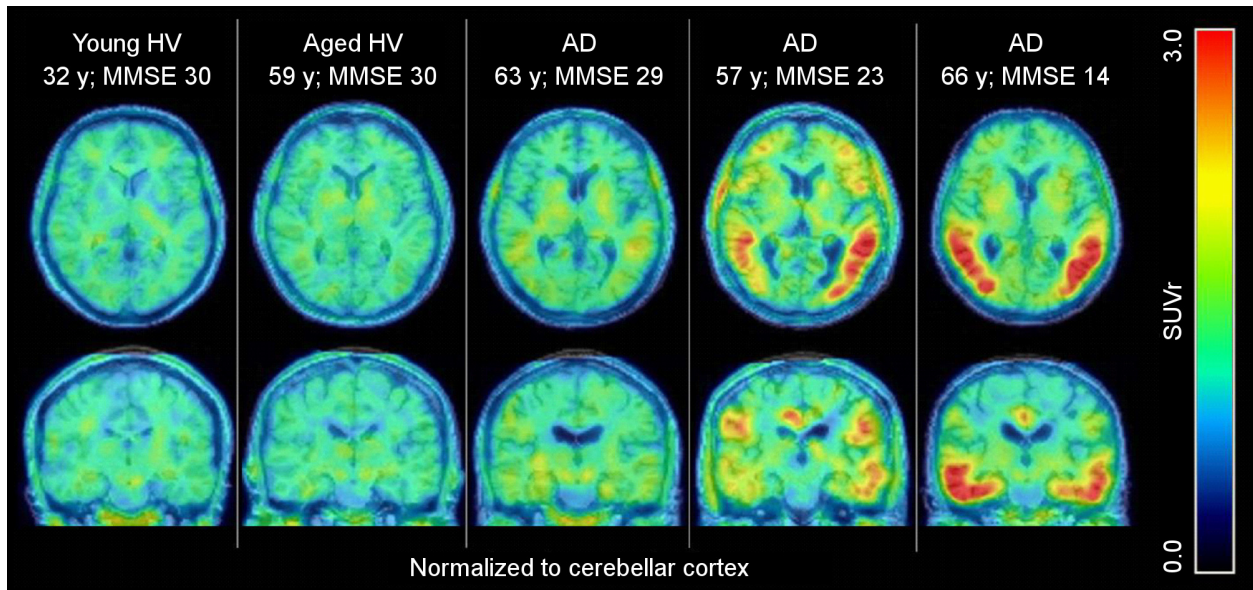


FIGURE 1. ^{18}F -AV-1451 SUVR images (80-100 min) superimposed onto the subject's MRI in transaxial (top row) and coronal (bottom row) views in one YHV, one AHV and three AD.

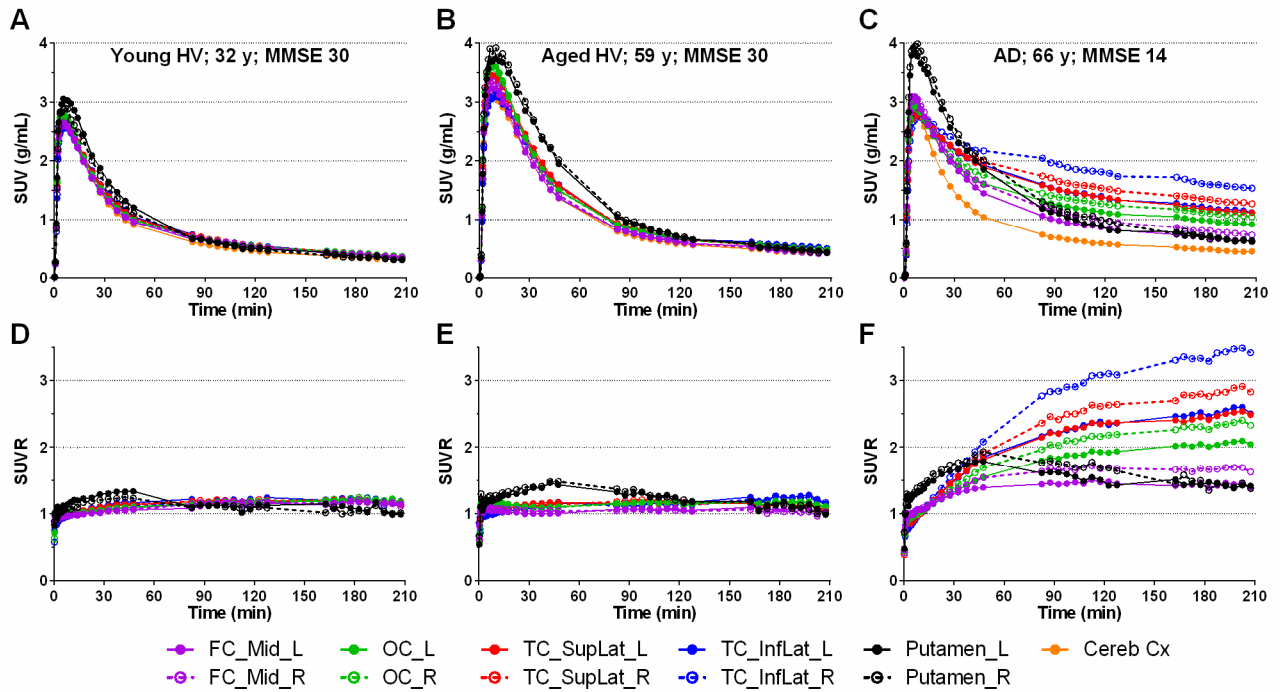


FIGURE 2. ^{18}F -AV-1451 time activity and SUVR curves in a young HV (A and D), an aged HV (B and E) and an AD (C and F). Closed symbols and solid lines= left side. Open symbols and dashed lines = right side. FC_Mid = Frontal middle cortex; OC = Occipital cortex; TC_SupLat = Superior lateral temporal cortex; TC_InfLat = Inferior lateral temporal cortex; Cereb Cx = Cerebellar cortex.

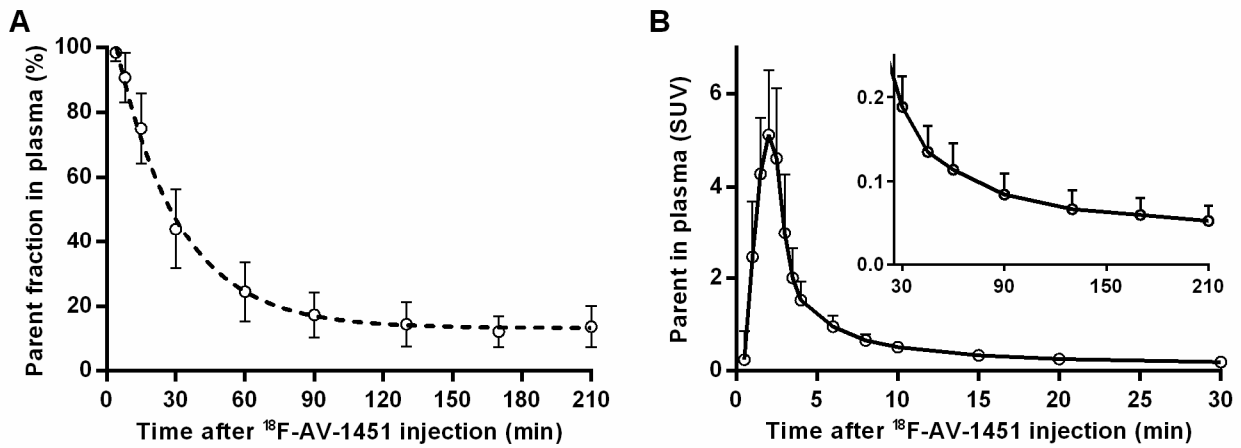


FIGURE 3. (A) Average (mean \pm SD) parent fraction profile in arterial plasma after intravenous administration of ^{18}F -AV-1451. Dashed line represents the monoexponential plus constant fit up to 130 min. (B) Average (mean \pm SD) radiometabolite corrected arterial plasma concentration of ^{18}F -AV-1451 (input function).

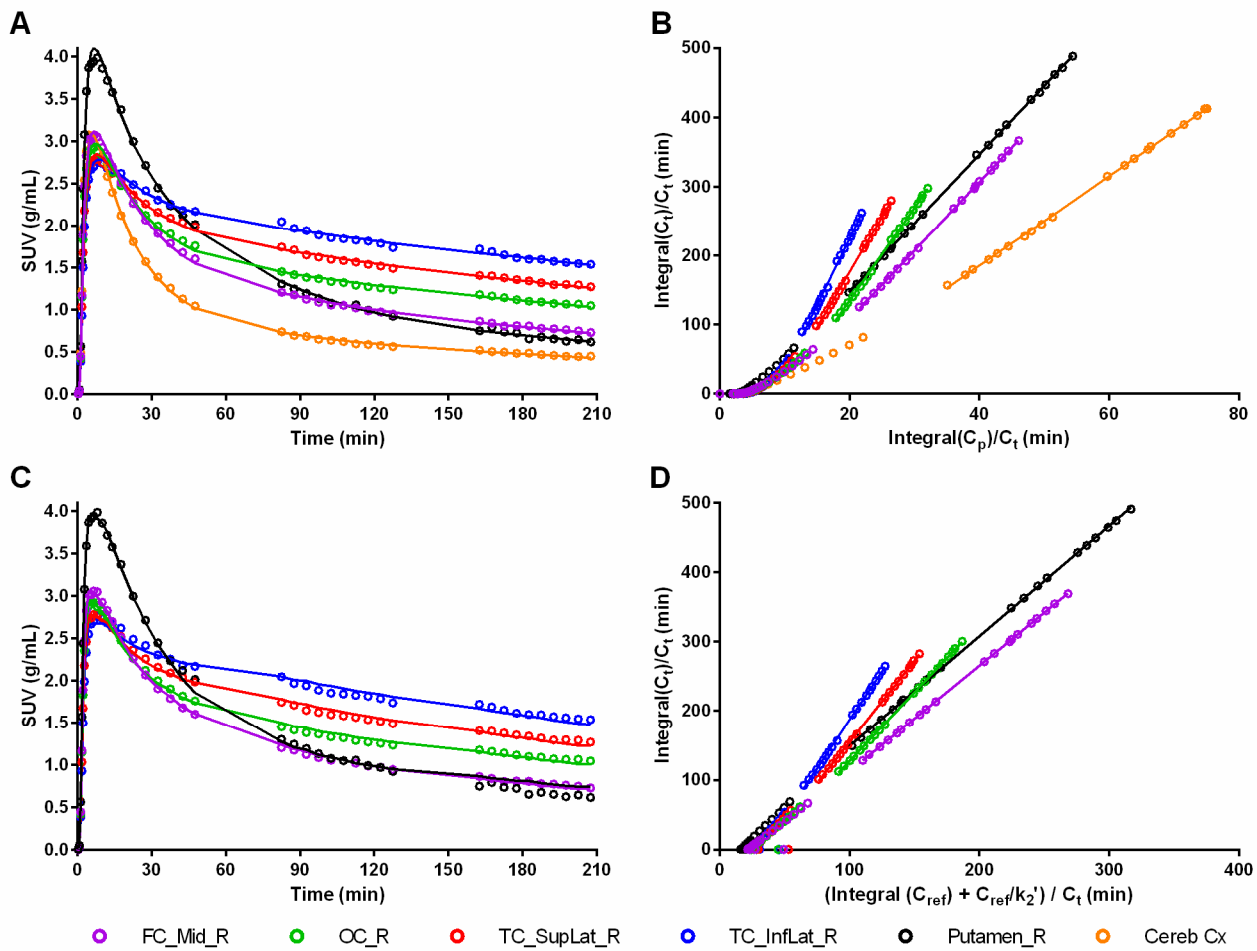


FIGURE 4. Compartmental and graphical analysis for an AD for 210 min of scanning data: (A) 2T fits, (B) Logan graphical analysis linear regression, (C) SRTM fits and (D) non-invasive Logan graphical analysis linear regression. Open symbols = measured data; Solid lines = fitted curve/line. FC_Mid = Frontal middle cortex; OC = Occipital cortex; TC_SupLat = Superior lateral temporal cortex; TC_InfLat = Inferior lateral temporal cortex; Cereb Cx = Cerebellar cortex.

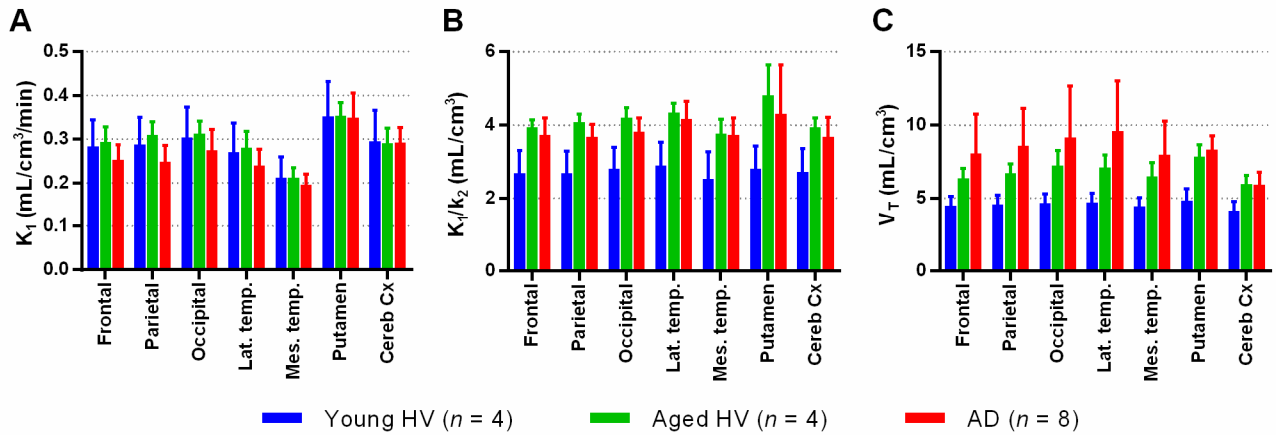


FIGURE 5. Two-tissue compartment model parameters using 130 min of scanning data.

Values are mean±SD within each group.

Average of left and right regions; Frontal = average of inferior, superior and middle; Lateral Temporal = average of superior and inferior.

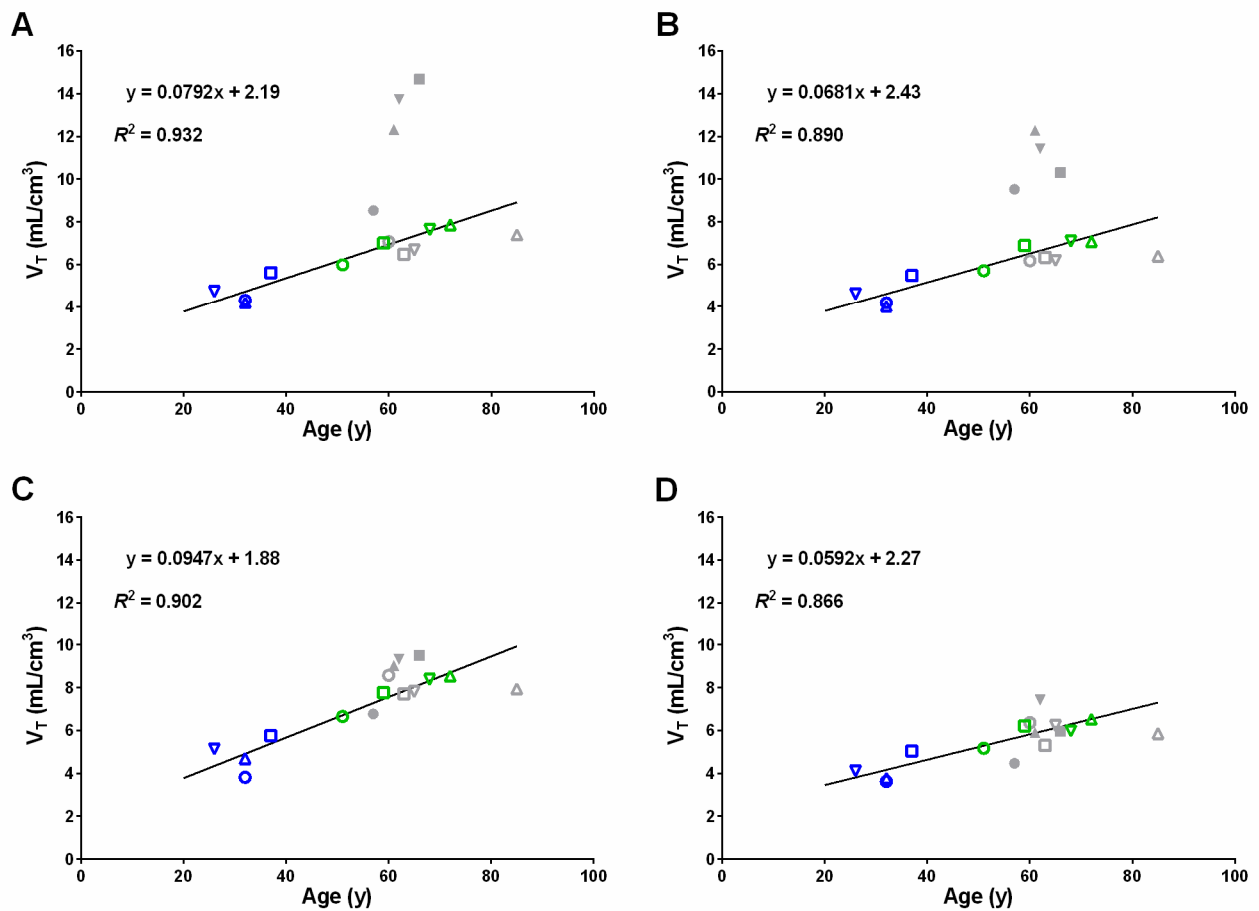


FIGURE 6. Linear regression of V_T (2T, 130 min) against the subjects age in A) lateral temporal cortex, B) parietal cortex, C) putamen and D) cerebellar cortex.

Blue symbols = Young HV; Green symbols = Aged HV; Solid line = linear regression.

AD (grey symbols) were excluded from the regression analysis, and are showed for information only:

open symbols = MMSE > 25 (low tau signal), closed symbols = MMSE < 25.

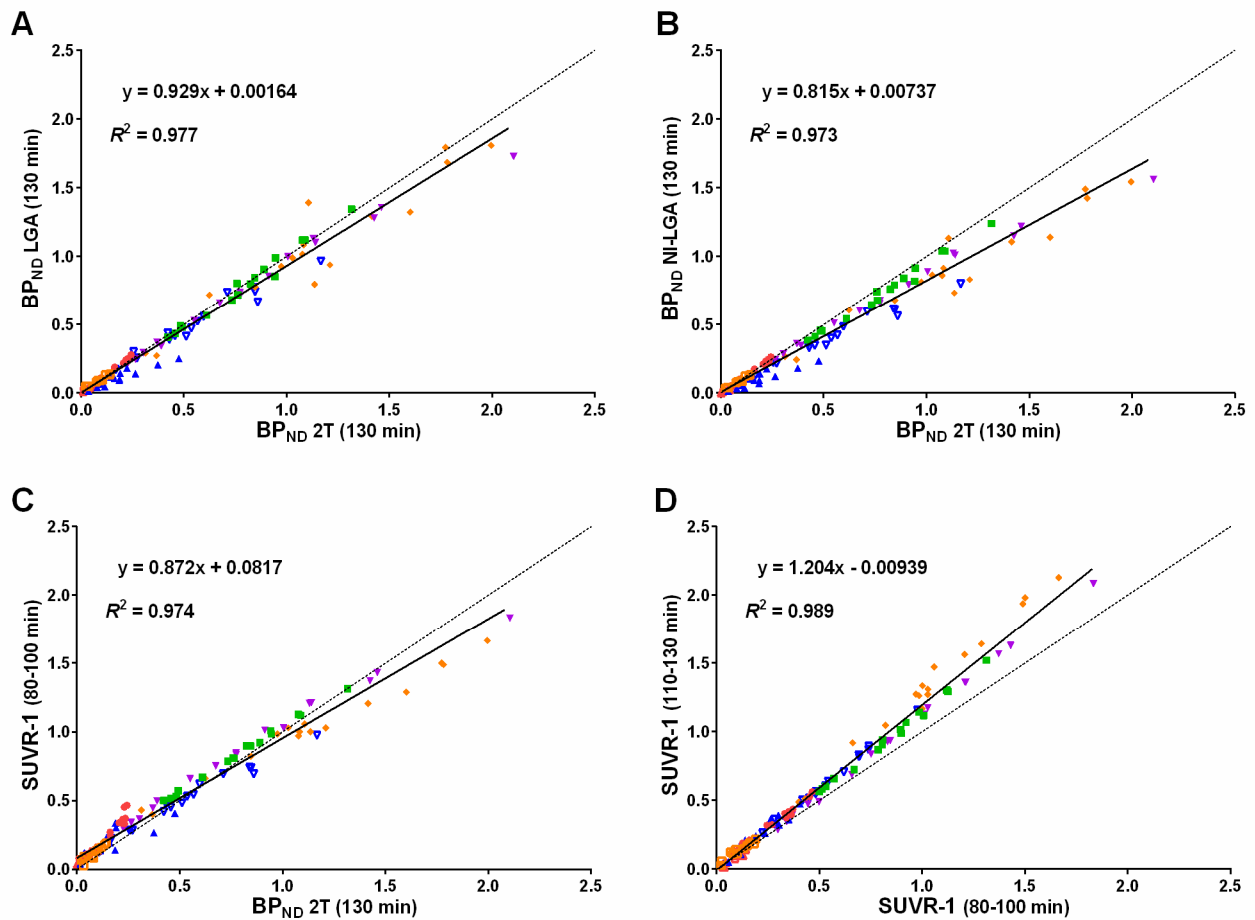


FIGURE 7. Regression analysis in AD (n=8) between BP_{ND} 2T (130 min) and (A) BP_{ND} LGA (130 min), (B) BP_{ND} NI-LGA (130 min) and (C) SUVR-1 (80-100 min), and (D) between SUVR-1 (80-100 min) and SUVR-1 (110-130 min). Colors indicate different subjects; solid line = linear regression; dashed line = line of identity.

TABLE 1. Demographics and Clinical Characteristics.

Characteristic	Young HV	Aged HV	AD
No. (% male)	4 (50%)	4 (50%)	8 (38%)
Age (y)	31.8±4.5 [26-37]	62.5±9.4 [51-72]	64.9±8.6 [57-85]
MMSE	30.0±0.0 [30]	29.5±0.6 [29-30]	22.4±5.5 [14-29]
CDR-SB	NA	NA	0.8±0.3 [0.5-1]
ADAS-cog	NA	NA	20.6±10.2 [4-30]
¹⁸ F-AV-1451 (MBq)	303.3±33.2 [259.6-340.4]	341.3±2.5 [338.5-344.5]	341.3±11.7 [325.4-357.0]
AV-1451 (µg)	0.49±0.13 [0.38-0.67]	0.82±0.59 [0.16-1.49]	0.58±0.46 [0.11-1.55]
¹⁸ F-florbetapir SUVR	NA	1.19±0.04	1.46±0.31

Values are mean±SD [range].

AD=Alzheimer's disease; HV=Healthy Volunteer; MMSE=Mini-Mental State Examination; CDR-SB=Clinical Dementia Rating, sum of boxes; ADAS-cog=Alzheimer's Disease Assessment Scale-Cognition; SUVR=standardized uptake value ratio; cerebellar cortex as reference; average of frontal, parietal, temporal, anterior and posterior cingulated cortex.

TABLE 2. Estimates of two-tissue compartment model parameters and macro parameters using 130 min of scanning data.

Group		Frontal	Parietal	Occipital	Lateral Temporal	Mesial Temporal	Putamen	Cerebellar Cortex
K ₁	YHV	0.28±0.06 (3±1%)	0.29±0.06 (3±1%)	0.30±0.07 (3±1%)	0.27±0.06 (3±1%)	0.21±0.04 (4±0%)	0.35±0.08 (5±1%)	0.30±0.07 (3±1%)
	AHV	0.29±0.03 (3±1%)	0.31±0.03 (3±1%)	0.31±0.03 (2±1%)	0.28±0.04 (2±1%)	0.21±0.02 (3±1%)	0.35±0.03 (3±0%)	0.29±0.03 (2±1%)
	AD	0.25±0.03 (2±1%)	0.25±0.04 (2±1%)	0.28±0.05 (2±1%)	0.24±0.04 (2±1%)	0.20±0.02 (2±1%)	0.35±0.06 (3±2%)	0.29±0.03 (2±1%)
K ₁ /k ₂	YHV	2.69±0.55 (4±1%)	2.69±0.57 (4±0%)	2.81±0.54 (4±0%)	2.89±0.58 (5±0%)	2.53±0.69 (8±3%)	2.82±0.64 (12±8%)	2.72±0.63 (4±0%)
	AHV	3.94±0.26 (4±1%)	4.08±0.21 (4±1%)	4.21±0.26 (3±1%)	4.35±0.26 (4±1%)	3.78±0.41 (6±2%)	4.82±0.88 (8±2%)	3.95±0.26 (4±1%)
	AD	3.73±0.50 (4±2%)	3.67±0.34 (4±2%)	3.82±0.38 (4±1%)	4.17±0.59 (5±2%)	3.73±0.46 (6±3%)	4.30±1.34 (9±6%)	3.69±0.53 (3±2%)
k ₄	YHV	0.023±0.010 (17±6%)	0.023±0.009 (15±5%)	0.022±0.007 (16±4%)	0.026±0.010 (17±6%)	0.032±0.019 (19±8%)	0.068±0.044 (15±4%)	0.029±0.014 (18±6%)
	AHV	0.017±0.005 (22±6%)	0.017±0.004 (21±3%)	0.014±0.004 (21±3%)	0.017±0.005 (23±5%)	0.020±0.010 (27±12%)	0.041±0.018 (19±18%)	0.019±0.007 (21±5%)
	AD	0.022±0.010 (11±8%)	0.020±0.008 (9±5%)	0.018±0.008 (10±7%)	0.020±0.009 (13±9%)	0.021±0.008 (16±10%)	0.044±0.018 (10±6%)	0.027±0.010 (12±8%)
k ₃ /k ₄	YHV	0.69±0.16 (10±2%)	0.73±0.18 (9±2%)	0.69±0.19 (9±2%)	0.65±0.15 (11±2%)	0.83±0.33 (15±5%)	0.77±0.38 (26±11%)	0.54±0.14 (12±3%)
	AHV	0.61±0.12 (9±2%)	0.64±0.10 (8±1%)	0.72±0.15 (8±2%)	0.63±0.12 (10±3%)	0.71±0.11 (17±6%)	0.65±0.16 (21±2%)	0.51±0.05 (9±3%)
	AD	1.16±0.65 (8±5%)	1.36±0.73 (7±4%)	1.41±0.89 (7±4%)	1.32±0.76 (9±5%)	1.15±0.54 (11±6%)	1.17±0.89 (16±7%)	0.62±0.20 (9±4%)
K ₁ k ₃ /k ₂ k ₄	YHV	1.79±0.21 (7±1%)	1.89±0.18 (6±1%)	1.88±0.25 (6±1%)	1.82±0.17 (8±1%)	1.91±0.23 (9±2%)	2.03±0.74 (14±4%)	1.42±0.10 (9±1%)
	AHV	2.43±0.55 (7±3%)	2.61±0.46 (7±2%)	3.05±0.75 (7±4%)	2.77±0.58 (8±4%)	2.71±0.55 (12±9%)	3.01±0.43 (14±4%)	2.03±0.33 (7±1%)
	AD	4.32±2.70 (5±4%)	4.90±2.60 (4±2%)	5.34±3.47 (5±3%)	5.44±3.30 (6±5%)	4.27±2.18 (6±4%)	4.03±1.12 (8±3%)	2.25±0.71 (5±3%)
V _T	YHV	4.49±0.62 (3±2%)	4.58±0.60 (2±1%)	4.68±0.57 (2±1%)	4.72±0.58 (2±2%)	4.45±0.58 (2±2%)	4.85±0.76 (1±0%)	4.14±0.64 (2±2%)
	AHV	6.37±0.73 (3±2%)	6.69±0.62 (3±1%)	7.26±0.95 (4±2%)	7.12±0.78 (4±2%)	6.48±0.89 (5±5%)	7.84±0.81 (2±2%)	5.98±0.58 (2±1%)
	AD	8.05±2.85 (2±2%)	8.58±2.52 (2±1%)	9.16±3.48 (2±1%)	9.62±3.42 (2±2%)	8.00±2.29 (3±2%)	8.34±0.92 (1±0%)	5.94±0.85 (1±0%)

Rate constants and macro parameters are presented as mean±SD and standard errors are expressed as percent and reported as (mean±SD).

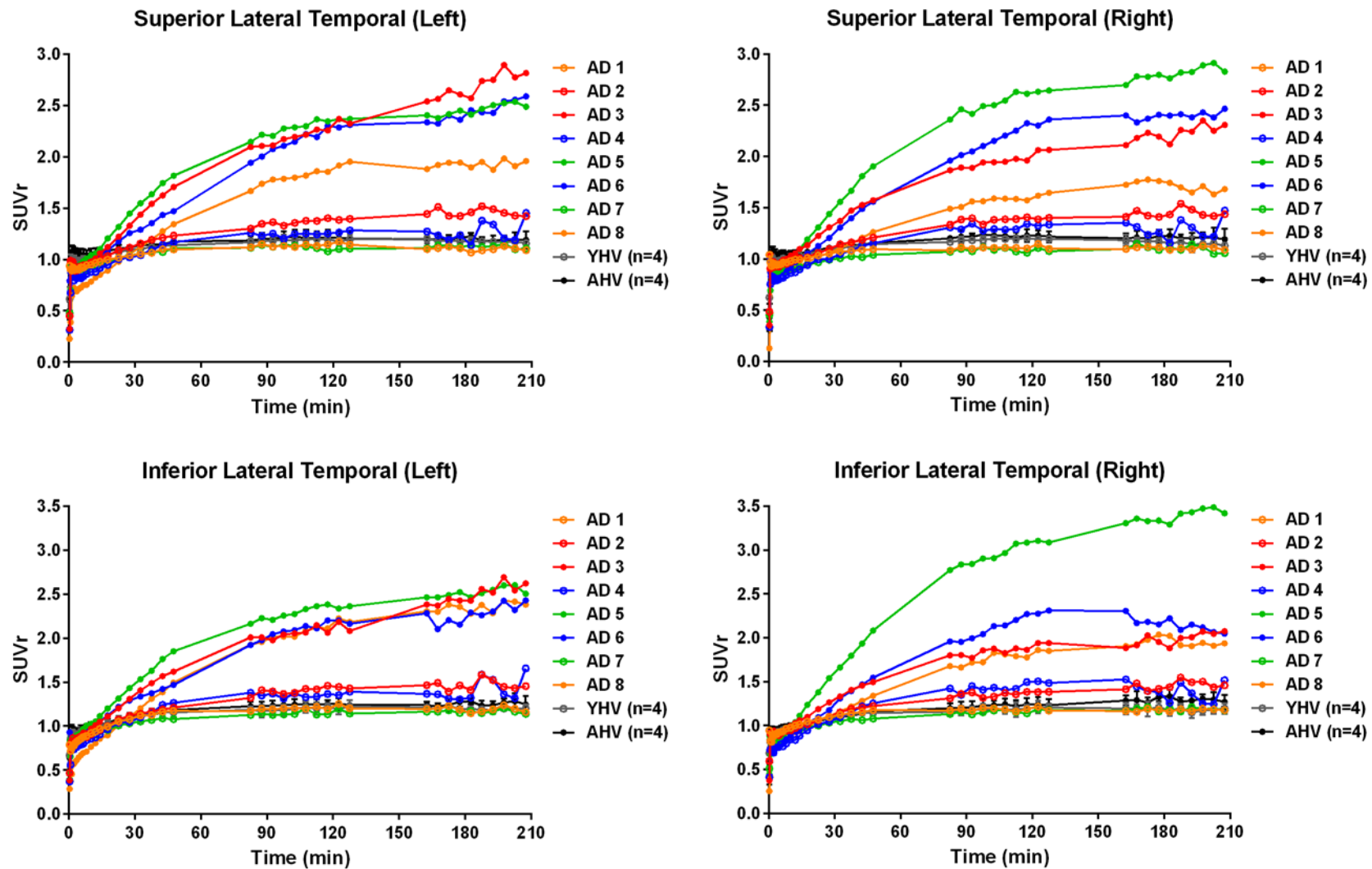
Average of left and right regions; Frontal = average of inferior, superior and middle; Lateral Temporal = average of superior and inferior.

YHV = Young Healthy Volunteer; AHV = Aged Healthy Volunteer; AD = Alzheimer's Disease subject.

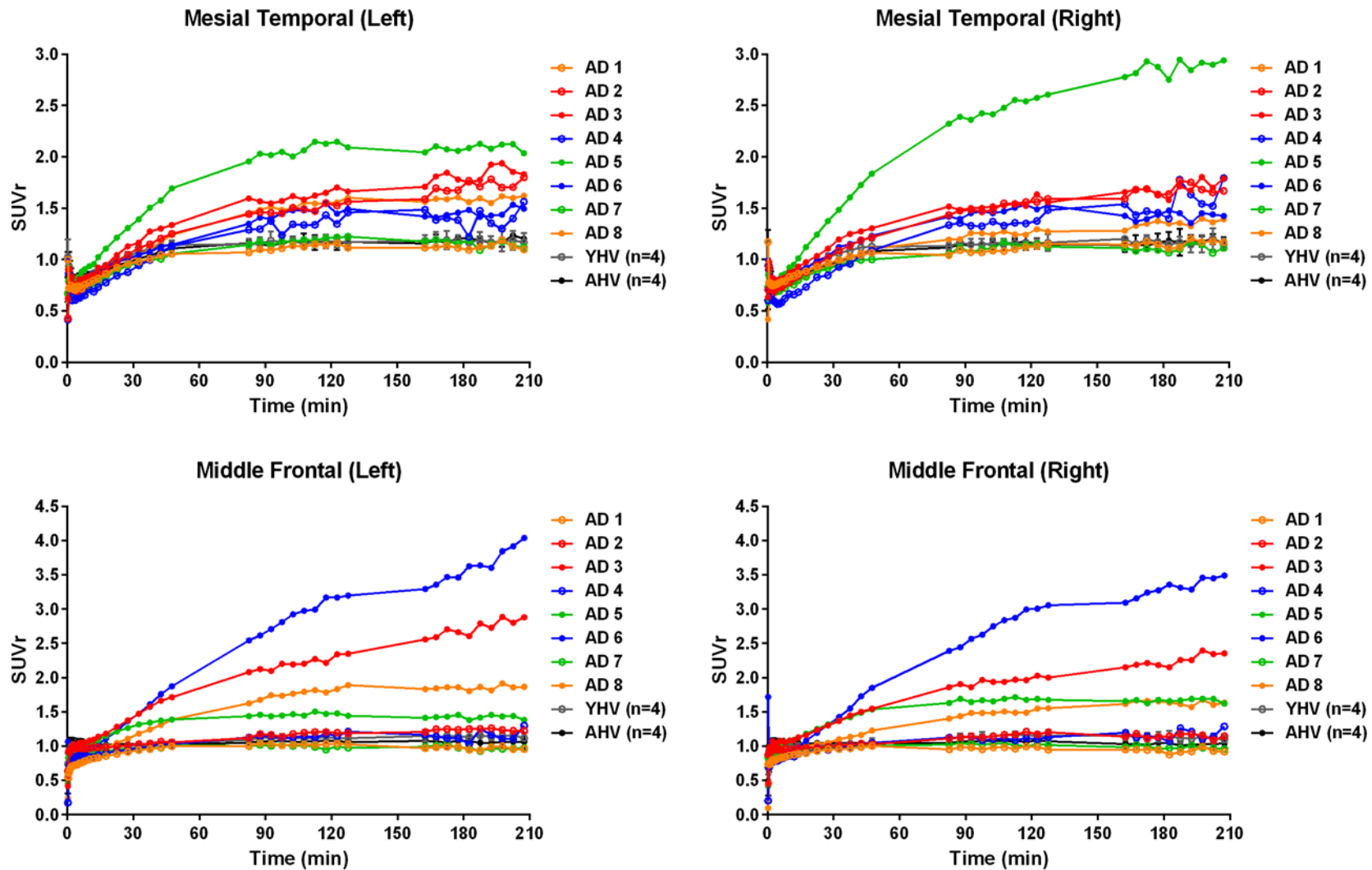
TABLE 3. Linear regression analysis of BP_{ND} and SUVR estimates across methods and scanning duration (130 and 210 min) in AD (n=8).

		2T	LGA	NI-LGA	SUVR-1 (80-100)	SUVR-1 (110-130)
2T	Slope	1.146	—	—	—	—
	Intercept	0.009	—	—	—	—
	R ²	0.95	—	—	—	—
LGA	Slope	0.929	1.103	—	—	—
	Intercept	0.002	0.003	—	—	—
	R ²	0.98	0.98	—	—	—
NI-LGA	Slope	0.815	0.887	1.123	—	—
	Intercept	0.007	0.007	0.005	—	—
	R ²	0.97	0.99	0.99	—	—
SUVR-1 (80-100)	Slope	0.872	0.943	1.069	—	—
	Intercept	0.082	0.092	0.083	—	—
	R ²	0.97	0.96	0.97	—	—
SUVR-1 (110-130)	Slope	1.088	1.145	1.289	1.204	—
	Intercept	0.081	0.089	0.080	-0.009	—
	R ²	0.97	0.98	0.98	0.99	—
SUVR-1 (160-180)	Slope	1.223	1.295	1.456	1.334	1.119
	Intercept	0.068	0.075	0.066	-0.036	-0.020
	R ²	0.96	0.97	0.97	0.96	0.97

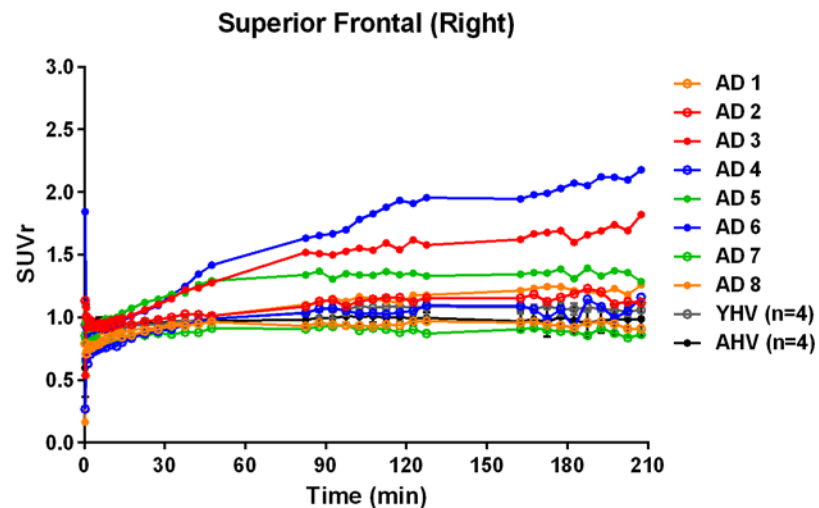
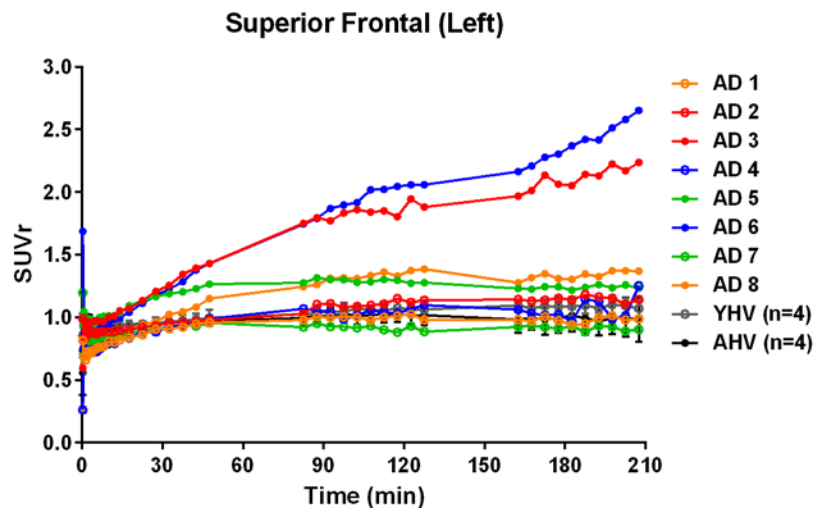
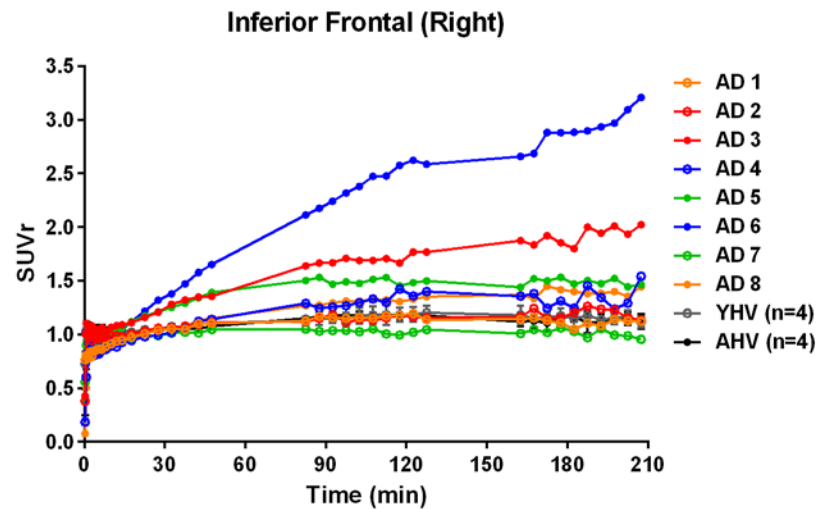
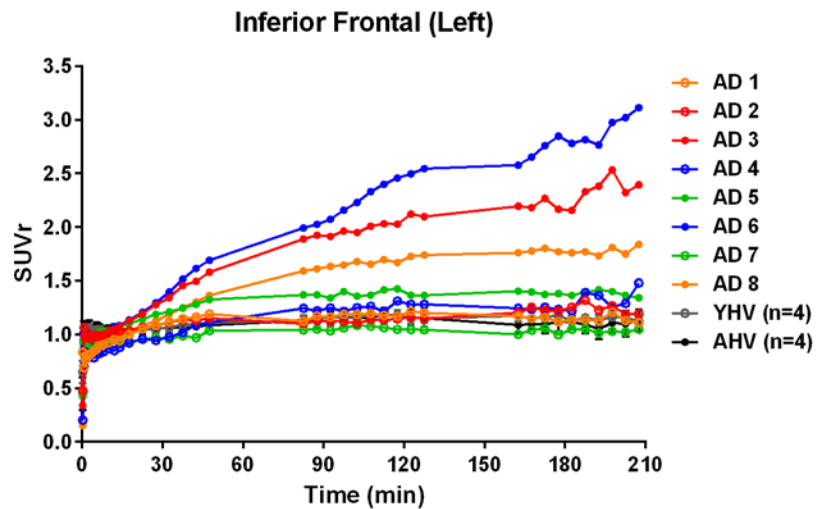
Below diagonal: column heading as abscissa and row heading as ordinate for 130 min estimates for 2T, LGA and NI-LGA. Diagonal: within method (2T, LGA and NI-LGA) comparison, 130 min estimates as abscissa and 210 min estimates as ordinate.



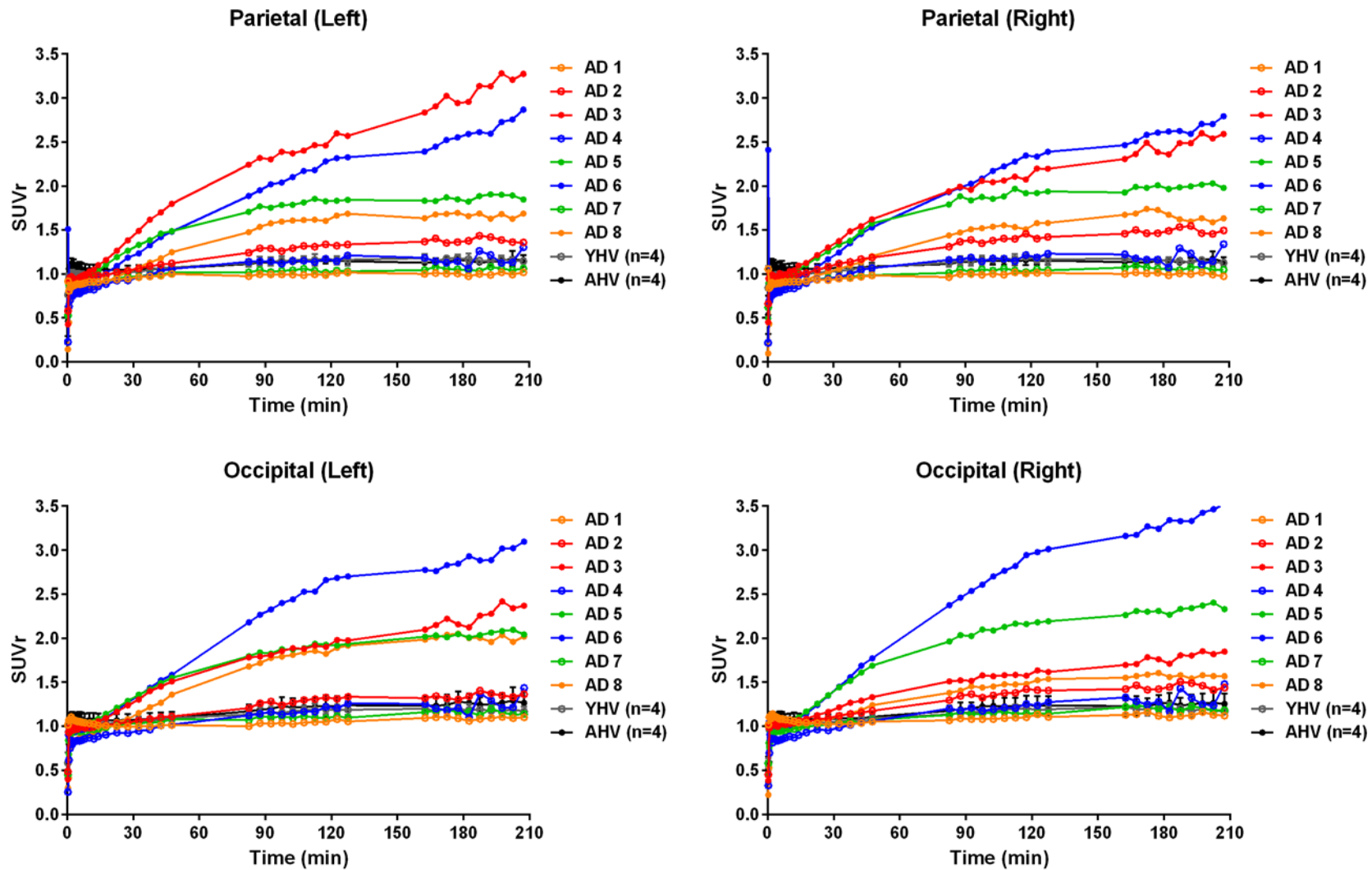
SUPPLEMENTAL FIGURE 1: ¹⁸F-AV-1451 SUVR curves in the superior and inferior lateral temporal cortex. Individual curves for the AD subjects and average curves (mean \pm SD) for the healthy volunteers are reported. AD = Alzheimer's Disease subject; YHV = Young Healthy Volunteer; AHV = Aged Healthy Volunteer.



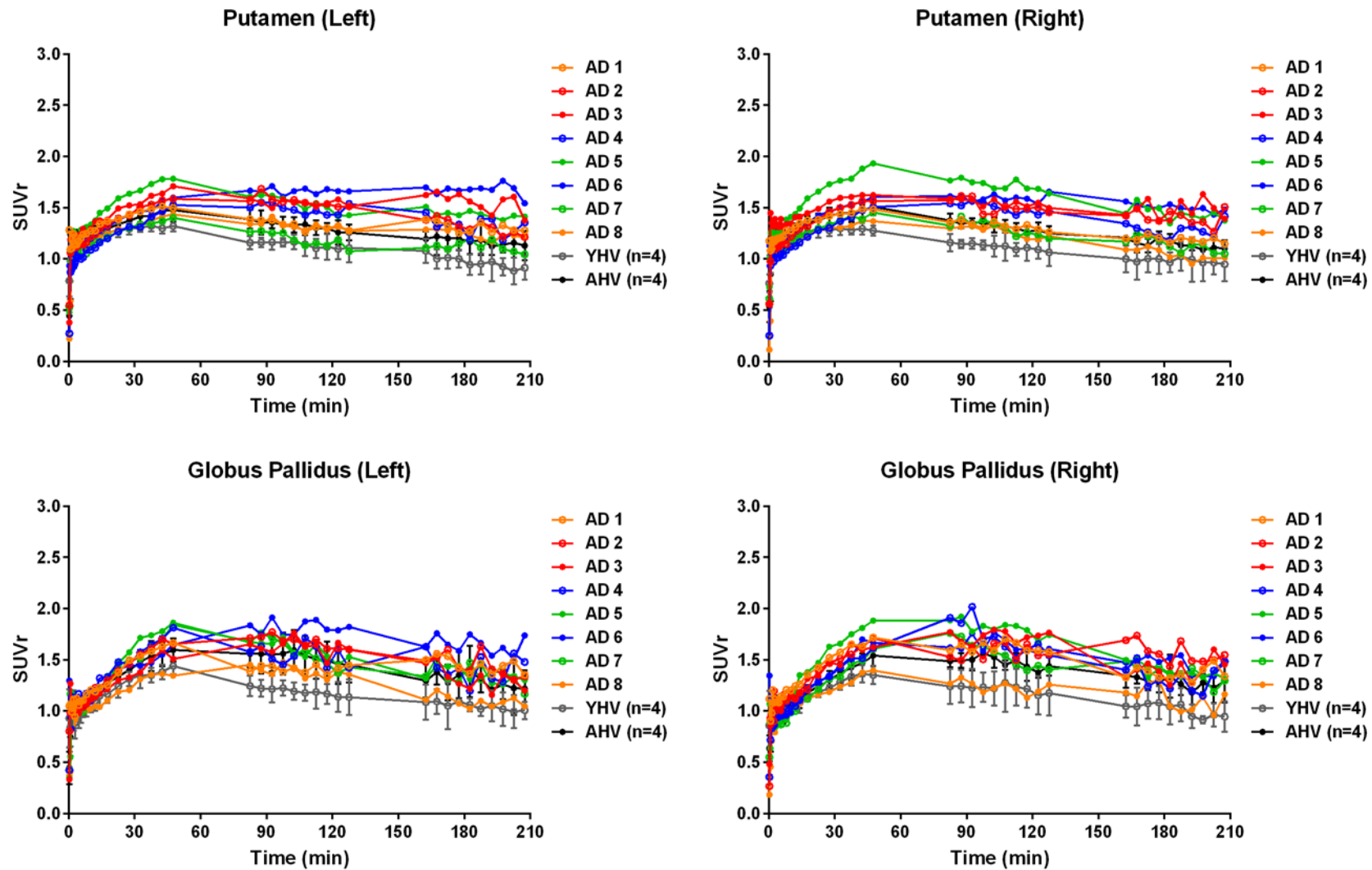
SUPPLEMENTAL FIGURE 2: ¹⁸F-AV-1451 SUVR curves in the mesial temporal cortex and the middle frontal cortex. Individual curves for the AD subjects and average curves (mean \pm SD) for the healthy volunteers are reported. AD = Alzheimer's Disease subject; YHV = Young Healthy Volunteer; AHV = Aged Healthy Volunteer.



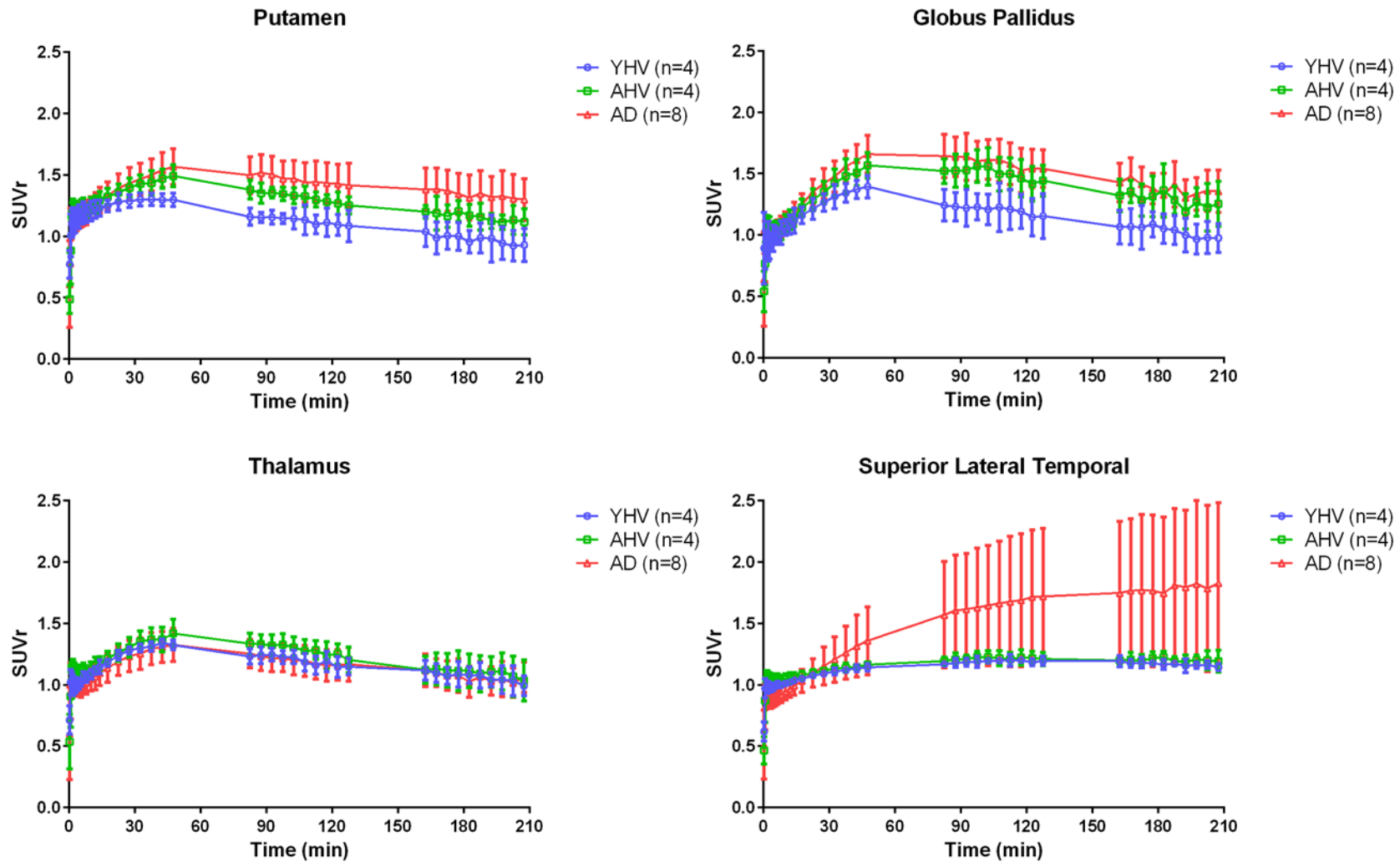
SUPPLEMENTAL FIGURE 3: ^{18}F -AV-1451 SUVR curves in the inferior and superior frontal cortex. Individual curves for the AD subjects and average curves (mean \pm SD) for the healthy volunteers are reported. AD = Alzheimer's Disease subject; YHV = Young Healthy Volunteer; AHV = Aged Healthy Volunteer.



SUPPLEMENTAL FIGURE 4: ¹⁸F-AV-1451 SUVR curves in the parietal cortex and the occipital cortex. Individual curves for the AD subjects and average curves (mean ± SD) for the healthy volunteers are reported. AD = Alzheimer's Disease subject; YHV = Young Healthy Volunteer; AHV = Aged Healthy Volunteer.



SUPPLEMENTAL FIGURE 5: ^{18}F -AV-1451 SUVR curves in the putamen and the globus pallidus. Individual curves for the AD subjects and average curves (mean \pm SD) for the healthy volunteers are reported. AD = Alzheimer's Disease subject; YHV = Young Healthy Volunteer; AHV = Aged Healthy Volunteer.



SUPPLEMENTAL FIGURE 6: Average (mean \pm SD) ^{18}F -AV-1451 SUVR curves in the putamen, globus pallidus, thalamus and superior lateral temporal cortex for the AD subjects and the healthy volunteers. AD = Alzheimer's Disease subject; YHV = Young Healthy Volunteer; AHV = Aged Healthy Volunteer.

SUPPLEMENTAL TABLE 1. Regional values of BP_{ND} (2T, LGA and NI-LGA; 130 min of scanning data) and SUVR estimates.

	Group	Frontal	Parietal	Occipital	Lateral Temporal	Mesial Temporal	Putamen
2T	YHV	0.08±0.07	0.11±0.04	0.13±0.04	0.14±0.04	0.08±0.04	0.17±0.09
	AHV	0.06±0.07	0.12±0.04	0.21±0.12	0.19±0.07	0.08±0.09	0.31±0.07
	AD	0.37±0.48	0.47±0.46	0.54±0.55	0.62±0.53	0.35±0.36	0.41±0.13
LGA	YHV	0.08±0.06	0.11±0.04	0.14±0.04	0.15±0.03	0.08±0.03	0.16±0.08
	AHV	0.06±0.06	0.12±0.04	0.18±0.08	0.17±0.04	0.06±0.04	0.30±0.07
	AD	0.36±0.48	0.45±0.46	0.51±0.50	0.55±0.46	0.32±0.33	0.38±0.13
NI-LGA	YHV	0.07±0.06	0.10±0.03	0.13±0.04	0.14±0.03	0.08±0.03	0.18±0.06
	AHV	0.05±0.06	0.11±0.03	0.16±0.07	0.16±0.04	0.05±0.04	0.33±0.07
	AD	0.31±0.42	0.40±0.42	0.45±0.43	0.50±0.42	0.29±0.30	0.40±0.12
SUVR-1 80-100	YHV	0.10±0.06	0.14±0.05	0.15±0.05	0.18±0.04	0.16±0.05	0.15±0.05
	AHV	0.08±0.07	0.13±0.03	0.20±0.07	0.21±0.05	0.15±0.03	0.36±0.06
	AD	0.39±0.42	0.49±0.43	0.52±0.46	0.63±0.46	0.43±0.34	0.50±0.14
SUVR-1 110-130	YHV	0.13±0.07	0.17±0.05	0.19±0.05	0.20±0.04	0.17±0.05	0.10±0.09
	AHV	0.08±0.08	0.15±0.04	0.23±0.10	0.23±0.06	0.16±0.05	0.28±0.07
	AD	0.47±0.54	0.59±0.52	0.64±0.57	0.73±0.54	0.51±0.38	0.43±0.17
SUVR-1 160-180	YHV	0.13±0.06	0.17±0.03	0.20±0.06	0.19±0.04	0.18±0.05	0.01±0.12
	AHV	0.05±0.09	0.14±0.03	0.24±0.10	0.24±0.06	0.16±0.05	0.19±0.08
	AD	0.51±0.62	0.68±0.62	0.73±0.64	0.79±0.61	0.55±0.44	0.37±0.17

Values presented as mean±SD.

Average of left and right regions; Frontal = average of inferior, superior and middle; Lateral Temporal = average of superior and inferior.

YHV = Young Healthy Volunteer; AHV = Aged Healthy Volunteer; AD = Alzheimer's Disease subject.